Available online at www.sciencedirect.com
ScienceDirect
Journal of Computational Physics 227 (2007) 1470–1482
JOURNAL OF COMPUTATIONAL PHYSICS
www.elsevier.com/locate/jcp

A multiscale approach to the analysis of magnetic grid shields and its validation

Oriano Bottauscio [a,*], Mario Chiampi [b], Alessandra Manzin [a], Paolo Emilio Roccato [b], Mauro Zucca [a]

[a] *Istituto Nazionale di Ricerca Metrologica (INRIM), Strada delle Cacce 91, 10135 Torino, Italy*
[b] *Dipartimento di Ingegneria Elettrica, Politecnico di Torino, Corso Duca degli Abruzzi 24, 10129 Torino, Italy*

Received 22 January 2007; received in revised form 24 April 2007; accepted 12 September 2007
Available online 21 September 2007

Abstract

This paper illustrates the application of the multiple scale expansion theory to the analysis of heterogeneous thin structures employed for the magnetic field shielding and, in particular, the attention is focused on grid shields. These structures are conveniently employed in the mitigation of magnetic fields when the thermal dissipation is a severe restriction. The problem modelling is faced by applying the thin-shell approximation to the Maxwell equations, introducing appropriate interface conditions between the shield surfaces. Starting from this formulation, a homogenisation technique, based on the multiple scale expansion theory, is developed in order to replace the heterogeneous structure with an equivalent homogenous one. The proposed method enables an efficient analysis of magnetic and pure conductive heterogeneous shields with a significant decrease of the computational burden. The results are validated by comparison with a standard modelling approach, when possible, and with experiments developed on specific laboratory set-ups for frequencies up to 2 kHz.

Keywords: Magnetic shielding; Multiscale problem; Homogenization technique; Thin-shell formulation

1. Introduction

Passive shields are largely employed for the mitigation of low frequency high power magnetic fields. To pursue this strategy, pure conductive or ferromagnetic sheets are arranged to form enclosures around the magnetic field sources, giving rise to significant shielding efficiencies in the surrounding area. A typical example is represented by cable enclosures, which enable a reduction of the magnetic field amplitude up to an order of magnitude. The main drawback of these solutions is a decrease of the thermal dissipation of the heat generated by Joule effect in the conductors. To avoid the consequent reduction of the cable ampacity, grid shields can be employed to limit the temperature increase.

* Corresponding author. Tel.: +39 011 3919828; fax: +39 011 3919849.
E-mail address: botta@inrim.it (O. Bottauscio).

0021-9991/$ - see front matter
doi:10.1016/j.jcp.2007.09.010

When standard approaches for electromagnetic field computations are applied to grid shields, two aspects concur to make the problem modelling arduous: the much reduced thickness of the shields and their fine periodic structure. The first difficulty is conveniently faced by the so-called *thin-shell* approach, which removes the three-dimensional screen by introducing suitable interface conditions between its surfaces [1,2]. The advantages of this technique have been extensively proved in several papers, evidencing its reliability in predicting the shielding efficiency of open and closed shields [3,4]. For what concerns the second aspect, grid shields exhibit a periodic structure that can be generated by the multiple repetition of a "basic cell". The geometrical properties of this basic cell influence the global behaviour of the shield, leading to a typical multiscale problem [5–7]. Being inconceivable to directly solve the problem with heterogeneous grid structures, the analysis can be advantageously handled by adopting a mathematical homogenization technique, which replaces the heterogeneous structure with an equivalent homogeneous one. This method, also suitable for the analysis of composite material sheets, is found to be able to well reproduce the electromagnetic field behaviour without unacceptable computational burdens [8].

This paper aims at coupling a homogenization technique, based on the multiple scale expansion theory, to the thin-shell formulation, in order to analyze the shielding efficiency of pure conductive or ferromagnetic grid sheets for low frequency magnetic field mitigation. The resulting numerical approach leads to the solution of an algebraic system composed of Finite Element (FE) relations, describing the interface conditions on the homogenized shell surface, and Boundary Element (BE) equations, accounting for the field distribution in the whole three-dimensional domain.

The originality of the mathematical model, described in Section 2, essentially consists in the fact that the multiple scale expansion theory is employed to directly deduce equivalent values of shield characteristic parameters. These parameters come from the application of the thin-shell approximation, implicitly involving the electric and magnetic material properties and also the shield thickness and the supply frequency.

The proposed numerical method is validated, comparing the computed results both with standard calculations performed on 2-D and 3-D heterogeneous structures (Section 3) and with measurements obtained in laboratory on 3-D grid shields (Section 4). The analysis, extended to pure conductive and ferromagnetic shields, in the frequency range from 50 Hz to 2 kHz, shows a very good agreement between computations and measurements. For higher frequencies, the discrepancies between measured and computed results increase. This can be explained taking into considerations that the thin-shell formulation is mainly able to model induced currents circulating in the shield plane. At the frequency increase, a significant portion of the induced currents tends to circulate in the shield thickness, affecting the shield efficiency [9].

2. Mathematical model

2.1. Three-dimensional problem

The electromagnetic field covers a three-dimensional open boundary air region, including the source conductors and a thin-shell. The shield surface is identified as domain $\Omega \subset \Re^2$, assuming a local coordinate system $s = (x_1, x_2)$. Under time-periodic supply conditions, the problem is formulated in the frequency domain, expressing the field quantities as phasors. Applying the thin-shell approximation, the following interface conditions between the shell faces (a) and (b) are found [1,10]:

$$-\nabla_S \cdot \left(\frac{1}{\sigma}\nabla_S \phi^{(-)}\right) = -\frac{i\omega\mu_0}{\sigma\xi}\left(H_{m,n}^{(+)} + 2\,H_n^{(s)}\right) \quad \text{in } \Omega \tag{1}$$

$$-\nabla_S \cdot \left(\zeta\nabla_S \phi^{(+)}\right) = -\mu_0 H_{m,n}^{(-)} - \nabla_S \cdot \left(2\zeta \boldsymbol{H}_t^{(s)}\right) \quad \text{in } \Omega \tag{2}$$

with $\gamma = (1+i)\sqrt{\omega\mu\sigma/2}$, $\zeta = \frac{\mu tgh(\gamma d/2)}{\gamma}$, $\xi = \frac{\gamma}{\sigma tgh(\gamma d/2)}$. In relationships (1) and (2) d is the shield thickness, σ and μ are the shield conductivity and permeability, ω is the angular frequency, i is the imaginary unit, ∇_S is the surface nabla operator, μ_0 is the air permeability, $\boldsymbol{H}^{(s)}$ is the external source field and $\boldsymbol{H}_m$ is the reduced curl-free field, whose tangential component is expressed as the gradient of the scalar potential ϕ. Symbols $(+)$ and $(-)$ indicate the sum and the difference between the values on sides (a) and (b), i.e.: $\phi^{(+)} = \phi^{(a)} + \phi^{(b)}$, $\phi^{(-)} = \phi^{(a)} - \phi^{(b)}$, $H_{m,n}^{(+)} = H_{m,n}^{(a)} + H_{m,n}^{(b)}$, and $H_{m,n}^{(-)} = H_{m,n}^{(a)} - H_{m,n}^{(b)}$.

Domain Ω is assumed to be highly periodic along x_1 and x_2 directions (Fig. 1). The spatial period Y is defined as the elementary cell, with a local coordinate system $y = s/\eta = (y_1, y_2)$ and area S_Y. Each cell is composed of an air region (material M1) and a pure conductive or ferromagnetic part (material M2). The assumption of a periodic structure implies that the magnetic permeability μ, the electrical conductivity σ and the derived parameters ζ and ξ are η-periodic functions: $\mu^\eta(s) = \mu(s/\eta)$, $\sigma^\eta(s) = \sigma\ (s/\eta)$, $\zeta^\eta(s) = \zeta(s/\eta)$ and $\xi^\eta(s) = \xi\ (s/\eta)$. The apex η underlines that the corresponding function depends on both the spatial coordinate system s ("global" variation) and the coordinate system y ("local" oscillations) defined on the element cell. Thus, introducing the weak formulation with a test function v, problems (1) and (2) become:

$$-\int_\Omega \frac{1}{\sigma^\eta}\nabla\phi^{\eta(-)}\cdot\nabla v\,\mathrm{d}s = -\mathrm{i}\omega\mu_0\int_\Omega \frac{\left(H^{\eta(+)}_{m,n} + 2H^{(\mathrm{s})}_n\right)}{\sigma^\eta\xi^\eta}v\,\mathrm{d}s \tag{3}$$

$$-\int_\Omega \zeta^\eta\nabla\phi^{\eta(+)}\cdot\nabla v\,\mathrm{d}s = -\mu_0\int_\Omega H^{\eta(-)}_{m,n}v\,\mathrm{d}s + 2\int_\Omega \zeta^\eta \boldsymbol{H}^{(\mathrm{s})}_t\cdot\nabla v\,\mathrm{d}s \tag{4}$$

In these equations the source field $\boldsymbol{H}^{(\mathrm{s})}$, which is obviously independent of the shield periodic structure, is not space periodic.

When $\eta \to 0$, that is when the cell number tends to infinite, the solutions of (3) and (4) converge weakly in $\mathcal{H} = \mathcal{H}^1_0(\Omega;\boldsymbol{C})$ to the corresponding solutions of the following "homogenized equations":

$$-\int_\Omega A^0\nabla\phi^{(-)}\cdot\nabla v\,\mathrm{d}s = -\mathrm{i}\omega\mu_0 M_Y\left(\frac{1}{\sigma\xi}\right)\int_\Omega \left(H^{(+)}_{m,n} + 2H^{(\mathrm{s})}_n\right)v\,\mathrm{d}s \tag{5}$$

$$-\int_\Omega B^0\nabla\phi^{(+)}\cdot\nabla v\,\mathrm{d}s = -\mu_0\int_\Omega H^{(-)}_{m,n}v\,\mathrm{d}s + \frac{2}{M_Y(1/\zeta)}\int_\Omega H^{(\mathrm{s})}_t\cdot\nabla v\,\mathrm{d}s \tag{6}$$

which provide the asymptotic behavior of $\phi^{\eta(-)}$ and $\phi^{\eta(+)}$ [11,12]. In Eqs. (5) and (6) symbol M_Y represents the average of the considered quantity on the elementary cell Y. A^0 and B^0 are, in the general case, 2×2 tensors, whose elements a^0_{ij} and b^0_{ij} are determined, following the energy method, as

$$\begin{cases} a^0_{ii} = \frac{1}{S_Y}\int_Y \frac{1}{\sigma}\,\mathrm{d}y + \frac{1}{S_Y}\int_Y \frac{1}{\sigma}\frac{\partial\chi_i}{\partial y_i}\,\mathrm{d}y & \text{with } i = 1,2 \\ a^0_{ij} = \frac{1}{S_Y}\int_Y \frac{1}{\sigma}\frac{\partial\chi_j}{\partial y_i}\,\mathrm{d}y & \text{with } i \neq j \end{cases} \tag{7}$$

$$\begin{cases} b^0_{ii} = \frac{1}{S_Y}\int_Y \zeta\,\mathrm{d}y + \frac{1}{S_Y}\int_Y \zeta\frac{\partial\kappa_i}{\partial y_i}\,\mathrm{d}y & \text{with } i = 1,2 \\ b^0_{ij} = \frac{1}{S_Y}\int_Y \zeta\frac{\partial\kappa_j}{\partial y_i}\,\mathrm{d}y & \text{with } i \neq j \end{cases} \tag{8}$$

Having denoted by $\mathcal{H}^1_{\mathrm{per}}(Y)$ the space of periodic functions in $\mathcal{H}^1(Y)$, functions $\chi_i \in \mathcal{H}^1_{\mathrm{per}}(Y)$ and $\kappa_i \in \mathcal{H}^1_{\mathrm{per}}(Y)$ are the solutions of the cell problems:

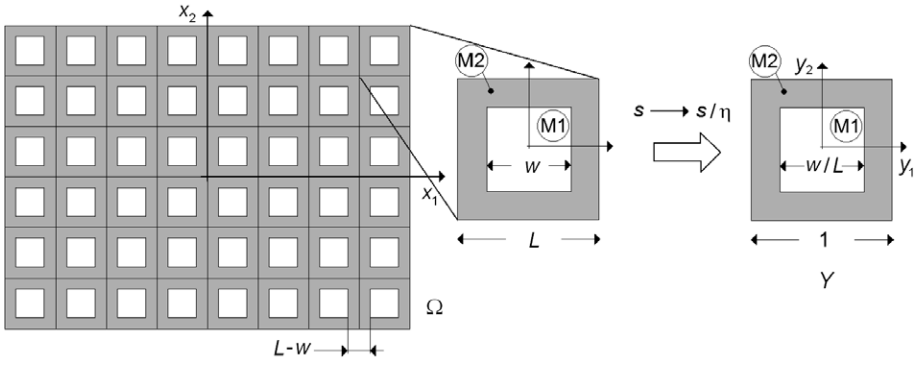

Fig. 1. Scheme of the grid shield with its elementary cell for the 3-D problem.

$$\begin{cases} \int_Y \frac{1}{\sigma}(\nabla\chi_i + \boldsymbol{e}_i)\cdot\nabla v\,\mathrm{d}y = 0 \quad \text{with } i = 1,2 \text{ for all } v \in \mathcal{H}^1_{\mathrm{per}}(Y) \\ \int_Y \zeta(\nabla\kappa_i + \boldsymbol{e}_i)\cdot\nabla v\,\mathrm{d}y = 0 \quad \text{with } i = 1,2 \text{ for all } v \in \mathcal{H}^1_{\mathrm{per}}(Y) \end{cases} \tag{9}$$

where $\boldsymbol{e}_1 = (1,0)$ and $\boldsymbol{e}_2 = (0,1)$ are the unit vectors along y_1 and y_2 directions. When considering elementary cells having geometrical symmetry with respect to both coordinate axes (y_1 and y_2), it results that $a^0_{21} = a^0_{12} = 0$, $b^0_{21} = b^0_{12} = 0$, $a^0_{11} = a^0_{22} = 1/\sigma^0$ and $b^0_{11} = b^0_{22} = \zeta^0$. Problems (9) are solved by the finite element method using first order shape functions and discretizing the domain Y (elementary cell) into triangles. An example of the spatial distribution of function χ_1, obtained for an elementary cell having $w/L = 0.5$, made of a pure conductive materials ($\sigma = 30\times10^6$ S/m) is shown in Fig. 2.

It is important to note that, since parameter ζ is frequency dependent, also the homogenized value ζ^0 depends on frequency.

2.2. Two-dimensional problem

Under 2-D approximation, the shield reduces to a segment lying in the (x_1x_3)-plane. A spatial periodicity is assumed on the segment, with an elementary period $Y = (-L/2, +L/2)$ (cell), whose central tract $(-w/2, +w/2)$ is composed of air (material M1) and the remaining part of material M2. Parameters σ, ζ and ξ assume the values σ_{M1}, ζ_{M1} and ξ_{M1} (resp. σ_{M2}, ζ_{M2} and ξ_{M2}) in material M1 (resp. M2).

Applying the homogenization process, the terms A^0 and $M_Y(1/\sigma\xi)$ in Eq. (5) become:

$$\begin{cases} A^0 = \frac{1}{M_Y(\sigma)} = \frac{L}{\sigma_{\mathrm{M1}}w + \sigma_{\mathrm{M2}}(L-w)} \\ M_Y\left(\frac{1}{\sigma\xi}\right) = \frac{1}{L}\left(\frac{w}{\sigma_{\mathrm{M1}}\xi_{\mathrm{M1}}} + \frac{L-w}{\sigma_{\mathrm{M2}}\xi_{\mathrm{M2}}}\right) \end{cases} \tag{10}$$

while the terms B^0 and $M_Y(1/\zeta)$ in Eq. (6) become:

$$\begin{cases} B^0 = \frac{1}{M_Y(1/\zeta)} \\ M_Y(1/\zeta) = \frac{1}{L}\left(\frac{w}{\zeta_{\mathrm{M1}}} + \frac{(L-w)}{\zeta_{\mathrm{M2}}}\right) \end{cases} \tag{11}$$

2.3. Integral equations and algebraic system

The homogenized equations (5) and (6), describing the interface conditions between shell faces (*a*) and (*b*), are discretized introducing a FE mesh on the shield surface (triangular elements), having assumed the

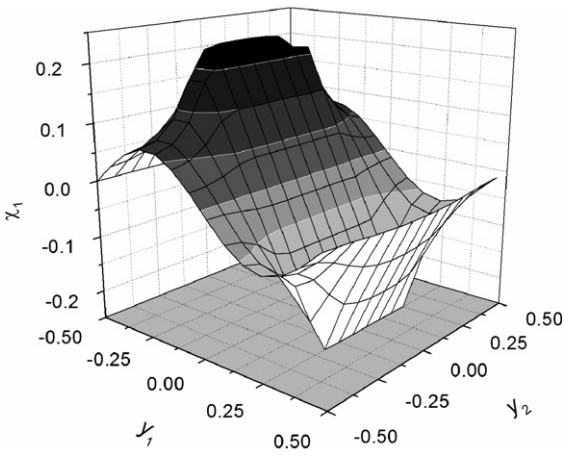

Fig. 2. Spatial distribution of function χ_1 for an elementary cell having a square hole ($w/L = 0.5$). The electrical conductivity and the relative permeability of material M2 are assumed equal to 30×10^6 S/m and 1, respectively.

unknowns $H_{m,n}^{(+)}$ and $H_{m,n}^{(-)}$ constant over each surface element and the unknowns $\phi^{(+)}$ and $\phi^{(-)}$ linear on the same element. The problem is completed by integral equations, describing the field in the open-boundary air region. For open shields these relationships are expressed by

$$\begin{cases} \frac{1}{2}\phi^{(+)} - \int_\Omega H_{m,n}^{(-)} \Psi \, \mathrm{d}s + \int_\Omega \phi^{(-)} (\nabla \Psi \cdot \boldsymbol{n}) \, \mathrm{d}s = 0 \\ \frac{1}{2} H_{m,n}^{(+)} + \int_\Omega H_{m,n}^{(-)} \nabla \Psi \, \mathrm{d}s \cdot \boldsymbol{n} + \int_\Omega \boldsymbol{n} \times H_{m,n}^{(-)} \times \nabla \Psi \, \mathrm{d}s \cdot \boldsymbol{n} = 0 \end{cases} \tag{12}$$

where Ψ is the Green function and $\boldsymbol{n}$ the outward normal unit vector to Ω. Similar expressions hold for closed shields [10]. Integral equation (12) are handled by the BE technique, using the surface discretization employed for the FE solution of problem equations (5) and (6).

3. Numerical validation

A first validation is carried out by comparing the proposed approach with a standard hybrid FE/BE model, directly applied to the heterogeneous structure, considering both 2-D and 3-D problems. The numerical solution of the heterogeneous structure by means of a standard approach requires a fine discretisation of the entire shield, able to resolve the local discontinuity of the material properties, strongly increasing the number of unknowns. As a consequence, in the case of 3-D structures, the reference heterogeneous solution provided by the standard method is available only when the computational burden is acceptable (pure ferromagnetic shield). In fact, for pure ferromagnetic shields, each finite element introduces approximately two real unknowns, while for conductive ones, the same element introduces four complex unknowns.

The aim of this analysis is devoted to evaluate the capability of the multiscale approach to reproduce the magnetic field behaviour in the case of a model problem, assuming idealized properties of the shield. The computation refers to a planar shield (1.2 m × 0.6 m) disposed 0.3 m over a go-and-return conductor system parallel to x_2 axis. The distance between the conductors is equal to 0.5 m (see Fig. 3). The grid shield, 3 mm thick, has the structure with square elementary cells presented in Fig. 1 and the origin of the coordinate system (x_1, x_2, x_3) is located in the shield centre.

In the 2-D simulations, the shield (width equal to 1.2 m) is assumed to be invariant along x_2 axis, so that the periodicity is only along x_1 axis. Keeping constant the global shield dimensions, the cell number N_c, the cell side L and the ratio w/L are varied. Of course, the condition $w/L = 1$ corresponds to the absence of the shield, while $w/L = 0$ identifies a solid shield, i.e. entirely made of material M2. In the considered cases material M2 can be a pure ferromagnetic ($\mu_r = 10{,}000$, $\sigma = 0$) or a pure conductive ($\mu_r = 1$, $\sigma = 30 \times 10^6$ S/m) medium. Due to the problem linearity, the computations have been performed assuming a unity current value.

In the 3-D simulations, the actual length of the shield (0.6 m) is accounted for. In this case, the influence of the geometrical parameters, controlled by ratio w/L, on the electromagnetic properties is well evidenced in the diagrams of Fig. 3, which reports the values of the homogenized electrical conductivity (σ^0) and relative

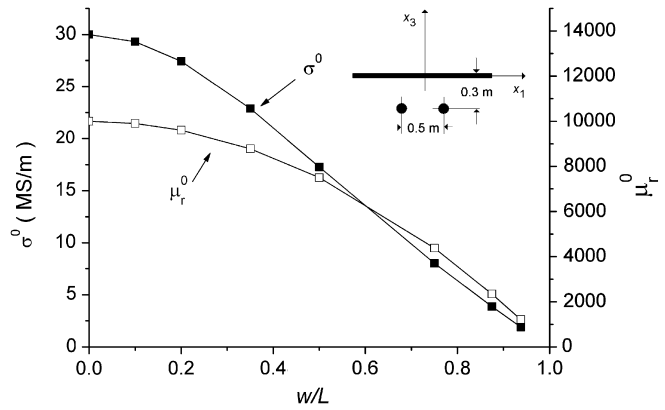

Fig. 3. Values of the homogenized electrical conductivity σ^0 (for a pure conductive material) and of the relative magnetic permeability μ_r^0 (for a pure ferromagnetic material) versus ratio w/L, for the considered 3-D structure. The shield arrangement is reported in the box.

magnetic permeability (μ_r^0), respectively for the pure conductive and the pure ferromagnetic materials. This result shows how the presence of holes in the shield structure weakly affects the shielding efficiency for values of w/L lower than ~0.2.

3.1. Pure ferromagnetic shield

For pure ferromagnetic shields, the reference numerical solution given by the standard approach applied to the heterogeneous shield is available for 2-D and 3-D structures. Having neglected the electrical conductivity, the analysis is developed under stationary supply conditions.

Under 2-D approximation, the shield structure is actually composed of ferromagnetic strips (material M2) directed along x_2-axis and separated each other by airgaps. This arrangement significantly limits the flow of magnetic flux along x_1 axis, reduces the shielding efficiency with respect to the actual 3-D structures and amplifies the local oscillations of the magnetic field, due to the material discontinuities. In Fig. 4 the magnetic field distributions computed along x_1 axis, at a distance of 0.1 m above the shield surface, are presented for cell numbers varying from 6 to 24. For a better understanding, the solution obtained with the solid shield is also reported. These results evidence how the approximation given by the homogenized solution improves at the increasing of the cell number. The local oscillations, particularly evident for low cell numbers (e.g. $N_c = 6$), are obviously neglected by the homogenization approach, which is specific for fine periodic structures.

In the 3-D computations, the agreement between the predictions of the homogenization technique and the reference results obtained directly considering the heterogeneous structure, is confirmed and even improved, as reported in Fig. 5. Again the accuracy of the homogenized solution increases when increasing the cell numbers, mainly for $w/L = 0.875$, where a more pronounced influence of the holes is found.

3.2. Pure conductive shield

Preliminary 2-D computations with a 400 Hz supply frequency show how, also for pure conductive shields, the heterogeneous solution tends to the homogenized one at the increase of N_c. This behavior is well evidenced in Fig. 6, where the magnetic field is plotted along x_1 axis, at a distance of 0.1 m from the shield surface. Moreover, the homogenization technique is able to satisfactorily reproduce the magnetic field, also varying the cell structure (ratio w/L), as shown by Fig. 7.

The 3-D analysis with homogenized parameters has been used to evaluate the effect of the hole dimensions on the shielding efficiency. The magnetic field distributions along x_1 axis at a distance of 0.2 m from the shield, presented in Fig. 8, prove that the effect of the holes becomes important only when the ratio w/L approaches to 1.

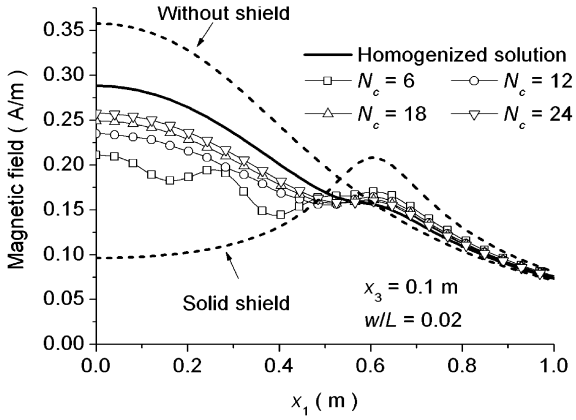

Fig. 4. Magnetic field along x_1 axis for a 2-D problem with a pure ferromagnetic shield having a variable number of cells with $w/L = 0.02$. The results corresponding to different values of N_c have been obtained applying a standard approach directly to the heterogeneous structure. The values are computed imposing a unity current in the conductors.

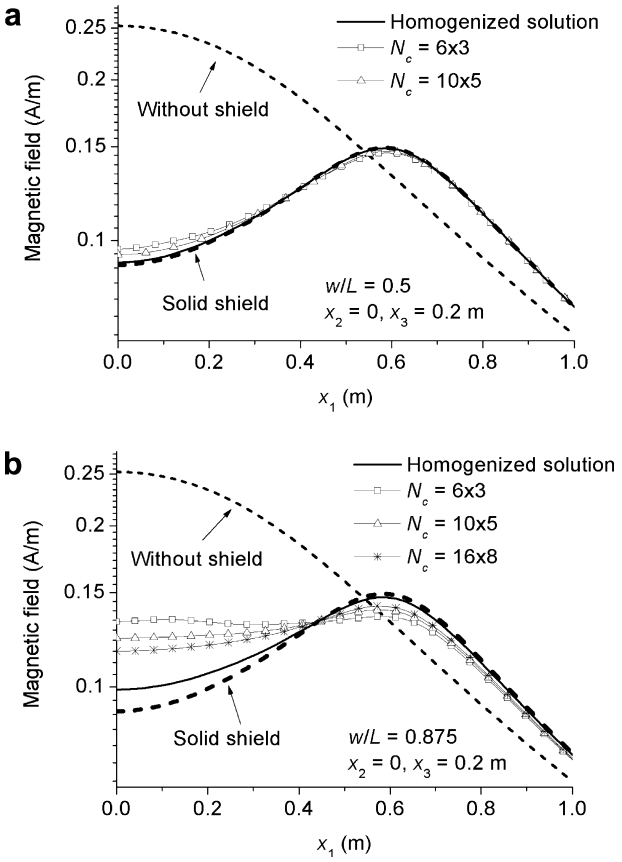

Fig. 5. Magnetic field along x_1 axis for a 3-D problem with a pure ferromagnetic shield having a variable number of cells with $w/L = 0.5$ (a) and $w/L = 0.875$ (b). The results corresponding to different values of N_c have been obtained applying a standard approach directly to the heterogeneous structure.

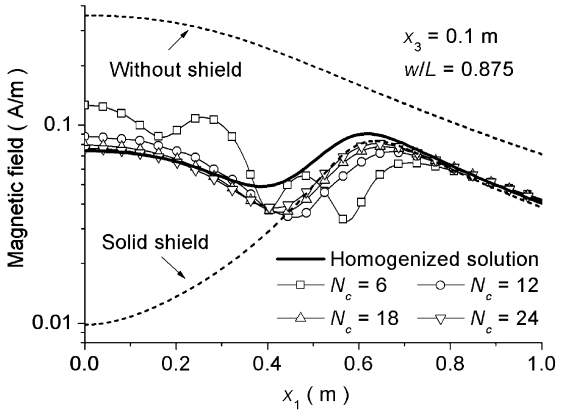

Fig. 6. Magnetic field along x_1 axis for a 2-D problem with a pure conductive shield having a variable number of cells with $w/L = 0.875$. The results corresponding to different values of N_c have been obtained applying a standard approach directly to the heterogeneous structure.

The 3-D numerical comparison with a standard solution of the heterogeneous structure has not been performed due to the significant increase of the unknowns in the heterogeneous shield problem. In fact, beside the above mentioned increase of problem unknowns for each finite element, a finer mesh is also required in order

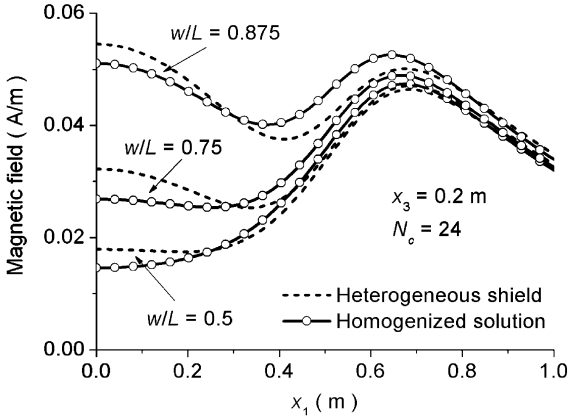

Fig. 7. Magnetic field along x_1 axis for a 2-D problem with a pure conductive shield having 24 cells and variable ratio w/L.

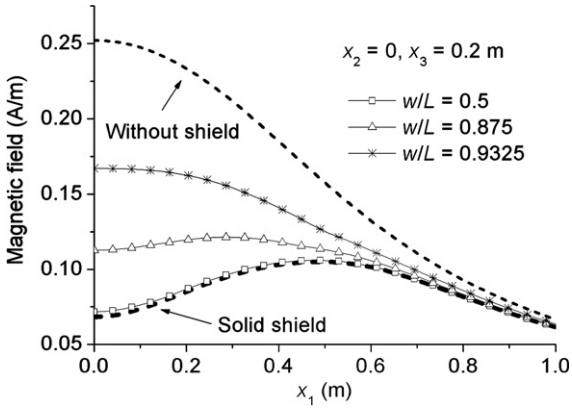

Fig. 8. Magnetic field computed along x_1 axis for the considered 3-D structure with a pure conductive shield with variable ratio w/L.

to well reproduce the strongly non-uniform eddy current distribution. Thus, in this case the validation is obtained only by comparison with experimental data.

4. Experimental validation

In the experiments the magnetic field is generated by a coil, whose axis is perpendicular to the shield surface (see Fig. 9). The coil, located at 30 mm from the shield, is supplied by a power amplifier. The laboratory set-up enables the generation of magnetic fields up to 1 mT in the investigation area, with a frequency ranging from 50 Hz to 2 kHz. The magnetic flux density is measured by means of an inductive field probe, having a sensitivity of 25 nT, with an accuracy of 5%. Different planar 2 m × 1 m grid shields are considered, disposing, in any case, the field probe at a minimum distance of 95 mm from the shield. Fig. 10 shows the structures of the ferromagnetic and pure conductive shields employed in the experimental analysis.

4.1. Ferromagnetic grid shield

Each analyzed shield is constituted of a 1.5 mm-thick Fe-C material (electrical conductivity $\sim 7.2 \times 10^6$ S/m, maximum relative permeability ~1500), with square holes arranged in a periodic way along the shield surface. As reported in Fig. 10, the two grids are composed of square elementary cells, having the same dimension of the internal hole ($w = 10$ mm), but different cell side L (grid step).

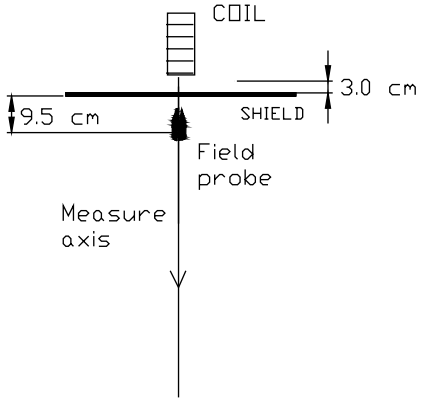

Fig. 9. Scheme of the 3-D grid shield with the coil (horizontal section).

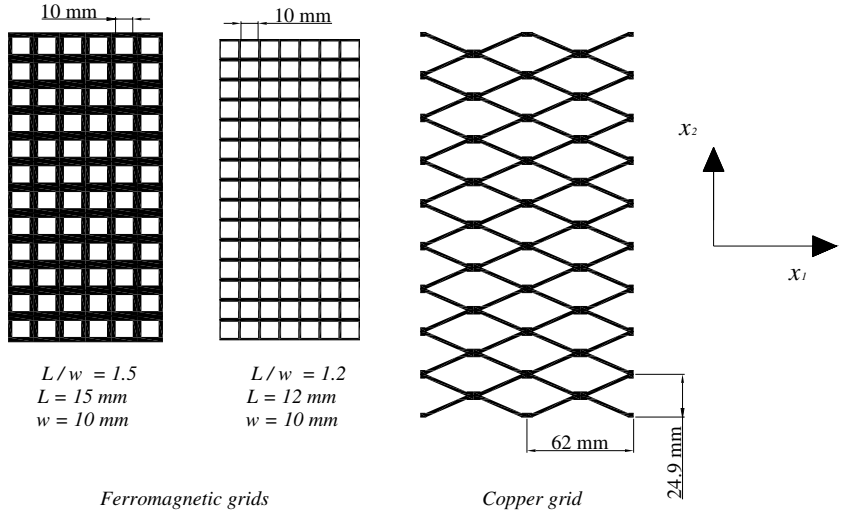

Fig. 10. Scheme of the Fe–C and copper grid shields considered for the experimental validation.

In the first set of computations and experiments, the dimension of the grid step is $L = 15$ mm. The corresponding values of the homogenized parameters are reported in Table 1, for two different supply frequencies. The distribution of the magnetic flux density amplitude along a line corresponding to the coil axis is shown in Fig. 11a and b, respectively for 50 Hz and 1 kHz supply frequency. A substantially good agreement is found between experiments and computations, proving the capability of the homogenization approach to deal with 3-D grid shields having ferromagnetic and conductive properties. Some discrepancies between computed and measured results are found only in close proximity of the shield, where the effects of the shield heterogeneities become stronger. Similar results are found for a shield having a different grid step ($L = 12$ mm), as shown in Fig. 12a and b.

Table 1
Homogenized values for the considered FE–C grid shield

f (Hz)	σ^0 (S/m)	ζ^0 (Re, Im) (H)	M_Y $(1/\sigma\xi)$ (Re, Im) (Ωm^2)	$M_Y(1/\zeta)$ (Re, Im) (H^{-1})
50	2.6×10^6	$(3.3 \times 10^{-7}, -1.3 \times 10^{-7})$	$(6.9 \times 10^{-4}, -1.4 \times 10^{-4})$	$(4.7 \times 10^8, 3.1 \times 10^5)$
1000	2.6×10^6	$(3.5 \times 10^{-8}, -1.2 \times 10^{-9})$	$(5.9 \times 10^{-4}, -1.7 \times 10^{-4})$	$(4.8 \times 10^8, 6.1 \times 10^7)$

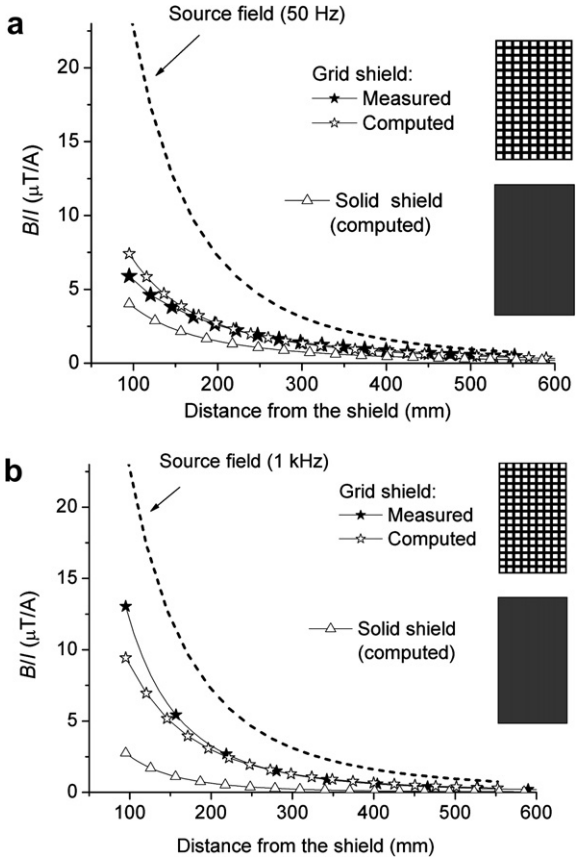

Fig. 11. Magnetic flux density amplitude B (values normalized to unity current amplitude I) along a line corresponding to the coil axis, for a Fe–C shield with $L = 15$ mm and $w = 10$ mm, and two values of the supply frequency: (a) 50 Hz, (b) 1 kHz. The field generated by the source, without shield, and the values obtained with a solid shield are also plotted for comparison.

The effect of the elementary cell dimensions on the shield efficiency is finally outlined in Fig. 13, making reference to the shielding factor SF, defined as the ratio $B_{\text{source}}/B_{\text{shield}}$, where B_{source} is the value of the magnetic flux density generated by the source and B_{shield} is the value reduced by the presence of the shield. The two curves, computed in a point at 95 mm from the shield, for a supply frequency of 50 Hz and 1 kHz, show the increase of SF at the increase of the dimension L of the elementary cell, keeping fixed w. Both curves tend to the limit value provided by a solid shield.

4.2. Conductive grid shield

The grid, whose structure is sketched in Fig. 10, is made of electrolytic copper, with conductivity equal to 58.5×10^6 S/m at 20 °C. As can be noted, this shield, having a non isotropic structure, shows a different behaviour along x_1 and x_2 directions. The comparison between experiments and computations has been performed for different values of the supply frequency (from 50 Hz to 2 kHz), the frequency being a parameter that strongly affects the efficiency of pure conductive shields. Fig. 14 reports the distribution of the magnetic flux density amplitude along the coil axis, for supply frequencies ranging from 500 Hz to 2 kHz. The results obtained at 50 Hz are omitted, the shield efficiency being negligible because of the reduced volume of conductive material. The agreement is satisfactory, considering the difficulties encountered in the experiments due to the increase of the temperature caused by the high Joule losses in the shield. The simulations have been performed using the electrical conductivity reported at the temperature reached by the shield during the experiments (44.5×10^6 S/m at ~120 °C).

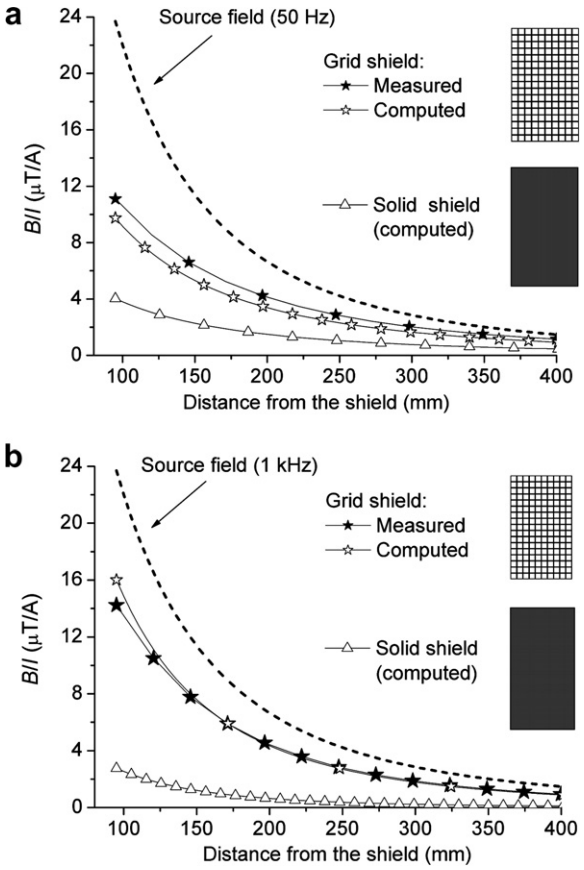

Fig. 12. Magnetic flux density amplitude B (values normalized to unity current amplitude I) along a line corresponding to the coil axis, for a Fe–C shield with $L = 12$ mm and $w = 10$ mm, and two values of the supply frequency: (a) 50 Hz, (b) 1 kHz. The field generated by the source, without shield, and the values obtained with a solid shield are also plotted for comparison.

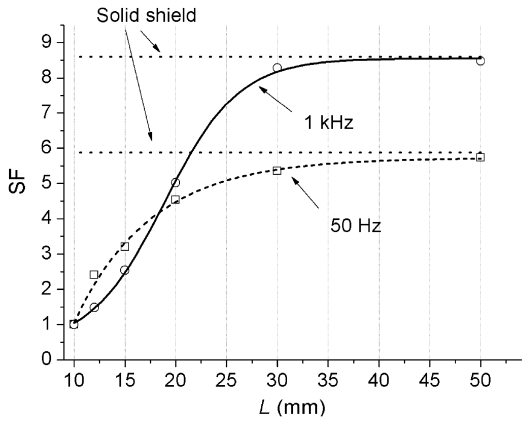

Fig. 13. Shielding factor SF computed at 95 mm from the shield for the considered Fe–C grid shield, varying the dimension L and keeping fixed the internal dimension $w = 10$ mm. The horizontal lines represent the results obtained with a solid shield.

The anisotropy of the grid structure influences the homogenized conductivity σ^0, whose value at 1.5 kHz varies from 7.1×10^6 S/m along x_1 axis to 1.3×10^6 S/m along x_2 axis. As direct consequence the shield efficiency is affected by the grid orientation. This is well demonstrated by the diagrams of Fig. 15, where a

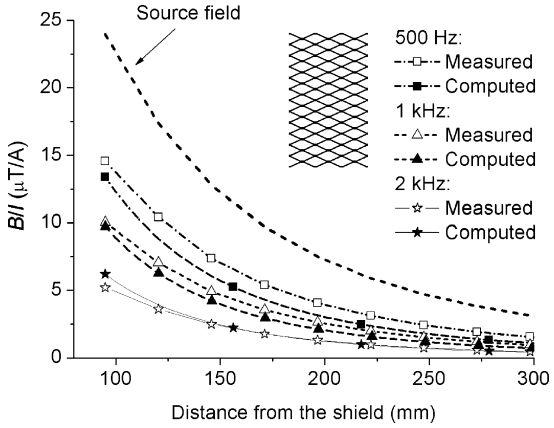

Fig. 14. Magnetic flux density amplitude B (values normalized to unity current amplitude I) along a line corresponding to the coil axis, for a copper shield having the structure of Fig. 11. The field generated by the source, without shield, is also plotted for comparison.

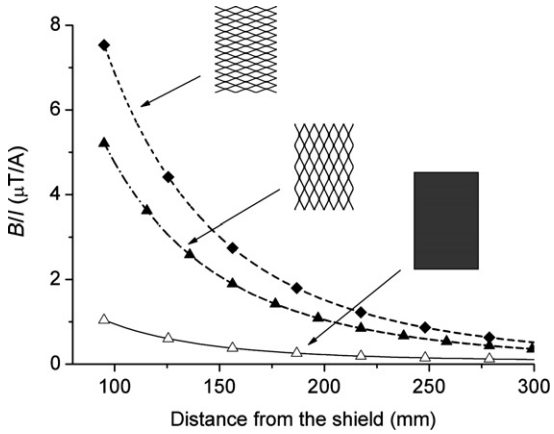

Fig. 15. Magnetic flux density amplitude B (values normalized to unity current amplitude I) computed along a line corresponding to the coil axis, for a copper shield having different orientation of the basic cell. The supply frequency is equal to 1.5 kHz. The field values, obtained with a solid shield, are also plotted for comparison.

rotation of the basic cell, with respect to the scheme of Fig. 10, determines an improvement of the shielding efficiency, considering that the shield length along x_2 axis is double with respect to the length along x_1 axis.

5. Conclusions

In this paper a numerical model, based on the multiscale expansion theory and on the *thin-shell* formulation, is developed and applied to the computation of the magnetic field mitigation produced by grid shields, conveniently employed when thermal dissipation is a severe restriction for the behaviour of the whole system.

The interest towards a modelling approach based on the homogenisation technique is justified by its capability to reproduce, with a limited computational effort, the shielding performances of complex 3-D grid structures, reducing the problem to the analysis of an equivalent homogeneous shield. The proposed method has been validated by comparison with a standard numerical procedure and with experiments performed on specific laboratory set-ups, considering shields with pure conductive or ferromagnetic properties. The experimental validation has evidenced that the effectiveness of the approach is good in the frequency range from d.c. to 2 kHz, which covers anyway most of the high power applications.

References

[1] I.D. Mayergoyz, Nonlinear Diffusion of Electromagnetic Fields, Academic Press, San Diego, 1998.
[2] L. Krähenbühl, D. Muller, Thin layers in electrical engineering. Example of shell models in analysing eddy-currents by boundary and finite element methods, IEEE Trans. Magn. 29 (1993) 1450–1455.
[3] O. Bottauscio, M. Chiampi, A. Manzin, Nonlinear ferromagnetic shield modeling by the thin-shell approximation, IEEE Trans. Magn. 42 (10) (2006) 3144–3146.
[4] H. Igarashi, T. Honma, A. Kost, A three-dimensional analysis of magnetic shielding with thin layers, in: Proceedings of the 7th IGTE Symposium on Numerical Field Calculation in Electrical Engineering, Graz, Austria, 1996, pp. 230–233.
[5] A. Bossavit, Effective penetration depth in spatially periodic grids: a novel approach to homogenization, in: International Symposium on Electromagnetic Compatibility, Rome, 13–16 September 1994, pp. 859–864.
[6] P. Kistenmacher, A. Schwab, Low-frequency shielding effectiveness of inhomogeneous enclosures, in: IEEE International Symposium on Electromagnetic Compatibility, 19–23 August 1996, pp. 347–352.
[7] H. Waki, H. Igarashi, T. Honma, Analysis of magnetic shielding effect of layered shields based on homogenization, IEEE Trans. Magn. 42 (4) (2006) 847–850.
[8] O. Bottauscio, V. Chiadò Piat, M. Chiampi, M. Codegone, A. Manzin, Electromagnetic phenomena in heterogeneous media: effective properties and local behaviour, J. Appl. Phys. 100 (4) (2006) 044902.
[9] O. Bottauscio, M. Chiampi, P.E. Roccato, M. Zucca, 1–100 kHz magnetic shielding efficiency by metallic sheets: modeling and experiment by a laboratory test bed, IEEE Trans. Magn. 42 (10) (2006) 3533–3535.
[10] O. Bottauscio, M. Chiampi, A. Manzin, Numerical analysis of magnetic shielding efficiency of multilayered screens, IEEE Trans. Magn. 40 (2) (2004) 726–729.
[11] E. Sanchez-Palencia, Non-homogeneous Media and Vibration Theory, Springer-Verlag, Berlin, 1980.
[12] D. Cioranescu, P. Donato, in: An Introduction to Homogenization, Oxford Lecture Series in Mathematics and its Applications, vol. 17, Oxford University Press, London, 1999.